

Calibration of a compact absolute atomic gravimeter

Hong-Tai Xie(谢宏泰), Bin Chen(陈斌), Jin-Bao Long(龙金宝), Chun Xue(薛春), Luo-Kan Chen(陈泺侃), Shuai Chen(陈帅)

Citation: Chin. Phys. B . 2020, 29(9): 093701 . **doi:** 10.1088/1674-1056/aba27b
Journal homepage: http://cpb.iphy.ac.cn; http://iopscience.iop.org/cpb

What follows is a list of articles you may be interested in

Movable precision gravimeters based on cold atom interferometry

Jiong-Yang Zhang(张炯阳), Le-Le Chen(陈乐乐), Yuan Cheng(程源), Qin Luo(罗覃), Yu-Biao Shu(舒玉彪), Xiao-Chun Duan(段小春), Min-Kang Zhou(周敏康), Zhong-Kun Hu(胡忠坤)

Chin. Phys. B . 2020, 29(9): 093702 . **doi:** 10.1088/1674-1056/aba9bc

Tilt adjustment for a portable absolute atomic gravimeter

Hong-Tai Xie(谢宏泰), Bin Chen(陈斌), Jin-Bao Long(龙金宝), Chun Xue(薛春), Luo-Kan Chen(陈泺侃), Shuai Chen(陈帅)

Chin. Phys. B . 2020, 29(7): 073701 . **doi:** 10.1088/1674-1056/ab90f9

Calibration of the superconducting gravimeter based on a cold atom absolute gravimeter at NIM

Qiyu Wang(王启宇), Jinyang Feng(冯金扬), Shaokai Wang(王少凯), Wei Zhuang(庄伟), Yang Zhao(赵阳), Lishuang Mou(牟丽爽), Shuqing Wu(吴书清)

Chin. Phys. B . 2018, 27(12): 123701 . **doi:** 10.1088/1674-1056/27/12/123701

Comparison of the sensitivities for atom interferometers in two different operation methods

Xiao-Chun Duan(段小春), De-Kai Mao(毛德凯), Xiao-Bing Deng(邓小兵), Min-Kang Zhou(周敏康), Cheng-Gang Shao(邵成刚), Zhu Zhu(祝竺), Zhong-Kun Hu(胡忠坤)

Chin. Phys. B . 2018, 27(1): 013701 . **doi:** 10.1088/1674-1056/27/1/013701

Precision measurement with atom interferometry

Wang Jin

Chin. Phys. B . 2015, 24(5): 053702 . **doi:** 10.1088/1674-1056/24/5/053702

SPECIAL TOPIC — Ultracold atom and its application in precision measurement

Calibration of a compact absolute atomic gravimeter*

Hong-Tai Xie(谢宏泰)[1,2,3], Bin Chen(陈斌)[1,2,3], Jin-Bao Long(龙金宝)[1,2,3], Chun Xue(薛春)[4], Luo-Kan Chen(陈泺侃)[1,2,3], and Shuai Chen(陈帅)[1,2,3,†]

[1] *Hefei National Laboratory for Physical Sciences at the Microscale and Department of Modern Physics, University of Science and Technology of China, Hefei* 230026, *China*

[2] *Shanghai Branch, CAS Center for Excellence in Quantum Information and Quantum Physics, University of Science and Technology of China, Shanghai* 201315, *China*

[3] *Shanghai Research Center for Quantum Sciences, Shanghai* 201315, *China*

[4] *Shanghai Division, QuantumCTek Co., Ltd. Shanghai* 201315, *China*

(Received 30 May 2020; revised manuscript received 28 June 2020; accepted manuscript online 20 August 2020)

Compact atomic gravimeters are the potential next generation precision instruments for gravity survey from fundamental research to broad field applications. We report the calibration results of our home build compact absolute atomic gravimeter USTC-AG02 at Changping Campus, the National Institute of Metrology (NIM), China in January 2019. The sensitivity of the atomic gravimeter reaches 35.5 μGal/$\sqrt{\text{Hz}}$ (1 μGal $= 1 \times 10^{-8}$ m/s^2) and its long-term stability reaches 0.8 μGal for averaging over 4000 seconds. Considering the statistical uncertainty, the dominant instrumental systematic errors and environmental effects are evaluated and corrected within a total uncertainty (2σ) of 15.3 μGal. After compared with the reference g value given by the corner cube gravimeter NIM-3A, the atomic gravimeter USTC-AG02 reaches the degree of equivalence of 3.7 μGal.

Keywords: atom interferometry, absolute gravimeter, systematic errors

PACS: 37.25.+k, 06.20.−f, 04.80.Nn **DOI:** 10.1088/1674-1056/aba27b

1. Introduction

The accurate measurement of the Earth's gravitational acceleration g is of great interest in modern science and technology, from fundamental research to wide applications in geophysics, geodesy, metrology as well as gravity assisted navigation.[1–4] As the value of g is both time and location dependent, compact gravimeters with high sensitivity and accuracy are required in a broad range of real field applications. The state-of-the-art absolute gravimeters based on optical interferometry and relative gravimeters are widely used at present time.[5–7] Based on the quantum technology of matter wave interferometry, the atomic gravimeters with potentially even higher sensitivity and stability are rapidly developing in the past two decades, and become new choices for precision g measurements.[8–19] Without any movable mechanical parts, the atomic gravimeters are more suitable for continuous running, working in outfield or on moving platforms.[16,20,21]

To measure g with high accuracy, the instruments and environment induced noises and systematic errors should be well evaluated and corrected. To verify the evaluation and correction results and assess the accuracy, comparisons or calibrations between absolute gravimeters are of great importance. For example, the International Comparison of Absolute Gravimeters (ICAG)[22–24] held every four years is the significant platform to evaluate the differences among various absolute gravimeters and to establish global absolute gravity reference at μGal (10^{-8} m/s^2) level. More and more atomic gravimeters participated in the comparisons and reached the degree of equivalence (DoE) from a few to tens of μGal,[10,15,25,26] proved to be reach the same level with the best performing optical-interferometry gravimeters with the test mass of the corner cube reflector (FG-5 and FG-5X).

Aiming towards the precision gravity measurements for field applications, we developed a compact atomic gravimeter USTC-AG02 based on cold atom matter wave interferometry in Shanghai Institute, University of Science and Technology of China (USTC). It was transported over 1300 km from Shanghai to the National Institute of Metrology (NIM), Beijing in January, 2019, to perform the gravity measurement and calibration. In the very quiet and clean precision gravity measurement lab at NIM, USTC-AG02 reached the sensitivity of 35.5 μGal/$\sqrt{\text{Hz}}$ and long-term stability of 0.8 μGal for averaging over 4000 seconds. After evaluating all the systematic effect induced by the gravimeter itself and correcting the influence by the environment, we obtained an uncertainty of 15.3 μGal (2 standard deviation) considering the statistical uncertainty. By comparing the measured g-values with the reference value offered by NIM, the degree of equivalence of

*Project supported by the National Key R&D Program of China (Grant No. 2016YFA0301601), the National Natural Science Foundation of China (Grant No. 11674301), Anhui Initiative in Quantum Information Technologies, China (Grant No. AHY120000), and Shanghai Municipal Science and Technology Major Project, China (Grant No. 2019SHZDZX01).

†Corresponding author. E-mail: shuai@ustc.edu.cn

© 2020 Chinese Physical Society and IOP Publishing Ltd

USTC-AG02 is calibrated as 3.7 μGal. It means that the compact atomic gravimeter USTC-AG02 can work as an absolute gravimeter with the accuracy in μGal level.

2. Compact atomic gravimeter USTC-AG02

The structure of our home build compact atomic gravimeter USTC-AG02 is presented in Fig. 1(a). It includes a cold atom sensor head (40 cm × 40 cm × 76 cm, 40 kg) and a mobile three-dimensional (3D) active vibration isolator (60 cm × 60 cm × 50 cm, 60 kg). An integrated controller package (56 cm × 68 cm × 72 cm, 80 kg) provides all the lasers for manipulating cold atoms, performing matter wave interferometry, detection, and data acquisition and processing. The total power consumption is less than 400 W. Figure 1(b) shows the atomic gravimeter USTC-AG02 in working.

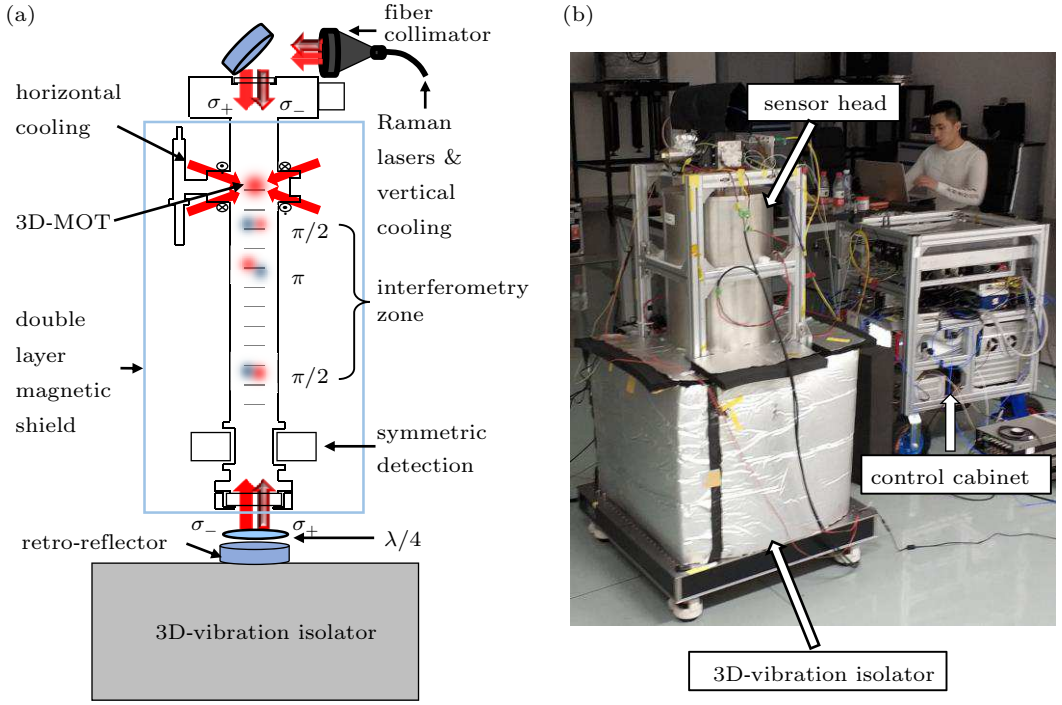


Fig. 1. (a) The schematic diagram of the sensor head of the compact atomic gravimeter USTC-AG02. (b) The photo of USTC-AG02 performing gravity measurement in NIM. It consist of a compact sensor head, a 3D vibration isolator, and a controller.

The sensor head consists of an ultra-high vacuum chamber filled with Rb atomic vapor at pressure of 10^{-9} mbar, optics for delivering laser beams, and photodiode detectors for collecting fluorescence signals. It is enclosed by a 3-layer μ-metal magnetic shield, with residual magnetic field below 20 nT in the whole interferometry region. A set of magnetic coils provide a quadrupole field for atom trapping and a homogeneous bias magnetic field for interferometry. The Raman interferometry lasers and the vertical cooling laser are combined and injected into the vacuum chamber through the fiber collimator from the top, and retro-reflected by a high quality mirror fixed on the 3D active vibration isolator. The additional four horizontal cooling lasers shine in the vacuum chamber at the three-dimensional magneto-optical trap (3D-MOT) area. The probe lasers are shining in the detection zone and the resonance fluorescence of the atoms are collected by the photodiode detector mounting symmetrically besides the vacuum chamber.

A homemade compact 3D active vibration isolator underneath the sensor head is applied to isolate the retro-reflected mirror from the ground vibration. It is based on a commercial passive isolation platform (Minus-K, 50BM-4), with eight voice coil motors mounted on symmetric positions in x, y, and z directions, respectively. A precision three-axis seismometer (Guralp CMG-3ESP) mounted on the isolation platform is applied to take the vibration noise signal of the retro-reflector. The noise signal goes through a programmable filter and the generated error signal is amplified to drive the voice coils for stabilizing the retro-reflector in three dimensions actively. The residual noise in vertical direction can be reduced by three orders of magnitude.[27]

All the lasers for operating the atomic gravimeter, including the cooling laser, repump laser, Raman lasers for interference, as well as the detection lasers are provided by the laser module that includes two diode lasers (DL-I and DL-II) and a tapered amplifier (TA). DL-I is locked on ^{87}Rb transition line by the magnetic enhanced modulation transfer spectroscopy,[28] providing repump laser and one of the Raman lasers. The laser from DL-II is amplified by the TA and phase locked to DL-I with the frequency offset near 6.835 GHz, providing cooling, probe, and the other Raman laser. The frequency of the functional lasers as well as the light

switches are controlled by a series of acousto-optic modulators (AOM). The lasers, optical components, and opto-electro elements are all integrated in a sealed module (46 cm × 42 cm × 15 cm) to improve the mechanical stability and compactness. The electronics for the laser controllers, power supplies, time controller, and data acquisition and processing units are installed in three standard 3U 19 inches electronic-boxes and mounted together with the laser module in the controller package. The output lasers are delivered to the sensor head through polarization maintaining fiber cables. The phase locked Raman lasers and the vertical cooling laser are combined together and aligned carefully along vertical direction with a retro-reflected configuration (see Fig. 1(a)).

For a gravity measurement cycle, the ^{87}Rb atoms as test mass are loaded directly from the background vapor by the 3D MOT in 120 ms and further cooled down to 3 μK by polarization gradient cooling in 5 ms. After the cooling stage, the lasers and the gradient magnetic field are all switched off simultaneously and the cold ^{87}Rb atoms start to free fall. With a series of Raman π-pulses, about 10^6 atoms are prepared in the magnetic insensitive initial state $|F=1, m_F=0\rangle$ with temperature of 300 nK in vertical direction. The Mach–Zehnder type matter wave interferometry is realized by a sequence of $\pi/2$–π–$\pi/2$ Raman pulses with the interrogation time of $T=92$ ms and π-pulse length of $\tau=20$ μs. To prevent from the incoherent photon scattering, the Raman lasers are red detuned 700 MHz to the D_2 transition lines. The frequency of one of the Raman lasers is chirped around $\alpha \approx 2\pi \times 25.1$ MHz/s to compensate the Doppler shift of the falling atoms. The output phase accumulated from the interferometer is[9]

$$\Delta\Phi = (\boldsymbol{k}_{\text{eff}} \cdot \boldsymbol{g} - \alpha)T^2 + \Delta\Phi_{\text{others}}, \tag{1}$$

where $\boldsymbol{k}_{\text{eff}}$ is the effective wave vector of the Raman lasers, and $\Delta\Phi_{\text{others}}$ is the phase shifts induced by the noises and systematic errors.

After the interferometry, the atoms fall down to the detection zone and the atom numbers in $|2,0\rangle$ and $|1,0\rangle$ states are counted by collecting the fluorescence of each state, respectively. The probability of an atom found in $|2,0\rangle$ state is expressed as

$$P_{|2\rangle} = P_0 - \frac{C}{2}\cos\Delta\Phi, \tag{2}$$

where P_0 is the mean of $P_{|2\rangle}$, and C is the fringe contrast. By scanning the chirp rate α, the interferometry fringe can be obtained and the gravity value g can be obtained via full-fringe fitting.

3. Continuous gravity measurement

We transported the atomic gravimeter USTC-AG02 from Shanghai Institute, USTC to Changping Campus, the National Institute of Metrology for calibration in January, 2019. It had been carried by a miniVan and transported over 1300 km. The gravity measurement was performed in the lab for precision gravity measurements at NIM. After the reinstallation and adjustment, USTC-AG02 ran at a repetition rate of 3 Hz and gave a g-value every 32 seconds. The continuous g measurement over night on January 20th, 2019 is presented in Fig. 2(a). The tide of the Earth is calculated by the program T-soft with the tidal parameters input from the observation results of a superconducting gravimeter.[29] The residues are the comparison between the measured g-values of USTC-AG02 and the Earth's tide. We can see clearly that the measured values fit with the tide model well and the fluctuations of the residues are around ±10 μGal.

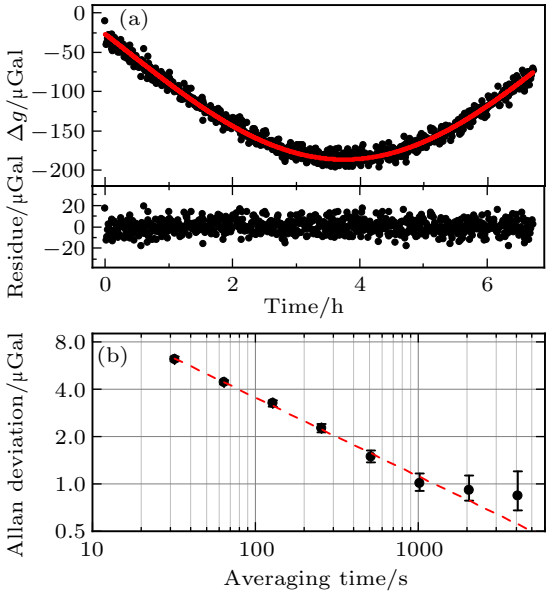


Fig. 2. Continuous g measurement at NIM, started from 2019-01-20T12:17Z. (a) Top: the black points indicate the g measurement data. Each datum is an average of 96 drops (32 seconds). The red curve indicates the Earth's tide. Bottom: the residues between the measurement data and the Earth's tide. (b) The black points and bars indicate the Allan deviations of the residues. The red line indicates the average expected for white noise.

The Allan deviations of the g measurement by our atomic gravimeter are represented in Fig. 2(b). The slope of the red line which is the fitting curve with $\tau^{-1/2}$ shows that the equivalent sensitivity at 1 second is 35.5 μGal. After averaging over 4000 s, the resolution is about 0.8 μGal.

The noise of the atomic gravimeter has been analyzed accordingly and the budget of the noises is given in Table 1. The residual phase noise from the Raman lasers is the dominated part, which gives the contribution of 28.2 μGal/$\sqrt{\text{Hz}}$ to the gravimeter. The detection noise is caused by the signal to noise ratio of the detected fluorescence signal, contributing a noise of 17.4 μGal/$\sqrt{\text{Hz}}$. Benefiting from the extremely quiet environment in Changping Campus, NIM, as well as the 3D active vibration isolator,[27] the vibration noise of the ground is greatly suppressed and only contributes 1.5 μGal/$\sqrt{\text{Hz}}$. Rest

of the noises including the magnetic field noise, laser frequency and intensity noise, are all small ones which are almost negligible in the present situation. From Table 1, the real noise in the measurement and the analyzed value fit well with each other.

Table 1. The noise budget of USTC-AG02.

Noise source	$\sigma_g/(\mu\text{Gal}/\text{Hz}^{1/2})$
Raman laser phase	28.2
Detection	17.4
Vibration	1.5
Magnetic field	0.7
Laser intensity noise	0.5
Laser frequency noise	0.5
Total	33.3
Experiment	35.5

4. Evaluation and correction of systematic errors

Systematic errors exist in the absolute gravimeters, and shift the measured g value. The phase shifts induced by systematic errors fall into two categories, either dependent ($\Delta\Phi_{\text{dep}}$) on or independent ($\Delta\Phi_{\text{ind}}$) of the direction of $\boldsymbol{k}_{\text{eff}}$.[30] The difference of the atomic phases accumulated along the two paths of the interferometer can thus be expressed as

$$\Delta\Phi = (\boldsymbol{k}_{\text{eff}} \cdot \boldsymbol{g} - \alpha)T^2 + \Delta\Phi_{\text{ind}} + \Delta\Phi_{\text{dep}}, \tag{3}$$

where $\Delta\Phi_{\text{ind}}$ includes the quadratic Zeeman shift, one-photon AC stack shift, radio-frequency phase shift, and light speed finite effect;[31] and $\Delta\Phi_{\text{dep}}$ mainly includes the tilt of the Raman lasers, two-photon light shift, Coriolis effect, self-attraction effect, gravity gradient effect, Raman laser's frequency shift, and wave-front abberation,[9,15,25] and so on. In this section, we present our analysis of USTC-AG02's systematic errors and a comparison between our measured g value and the reference value given by NIM.

4.1. Wave-vector independent errors

As presented in Fig. 1(a), the Raman lasers for interferometry have the retro-reflected structure. There are two pairs of counter-propagating lasers with the effective wave vector $\boldsymbol{k}_{\text{eff}}$ in opposite directions, as shown in Fig. 3(a). Due to the Doppler effect of the falling atoms, when we chirp the Raman lasers' frequency with a negative rate $-\alpha_{\text{u}}$ (or a positive rate $+\alpha_{\text{d}}$), $\boldsymbol{k}_{\text{eff}} > 0$ (or $\boldsymbol{k}_{\text{eff}} < 0$) is selected. During the g measurement procedure, the sign of the chirping rate α is switched in every 16 seconds, with 48 circles of interferometry. A pair of interference fringes with chirping rates of $-\alpha_{\text{u}}$ and $+\alpha_{\text{d}}$ are shown in Fig. 3(b). The extreme points of the two cosine fitting curves are separated, with $\alpha_{\text{u0}} = 2\pi \times 25123538.72 \pm 0.25$ Hz/s and $\alpha_{\text{d0}} = 2\pi \times 25123552.25 \pm 0.38$ Hz/s, respectively.

With the flip chirping approach, the phase shift from Eq. (3) becomes

$$\begin{aligned}(+k_{\text{eff}}g - \alpha_{\text{u0}})T^2 + \Delta\Phi_{\text{ind}} + \Delta\Phi_{\text{dep}} = 0,\\ (-k_{\text{eff}}g + \alpha_{\text{d0}})T^2 + \Delta\Phi_{\text{ind}} - \Delta\Phi_{\text{dep}} = 0.\end{aligned} \tag{4}$$

As we subtract these two formula, the wave vector independent phase shift $\Delta\Phi_{\text{ind}}$ is cancelled and only the $\Delta\Phi_{\text{dep}}$ term is left. The g value can be derived as

$$g = \frac{(\alpha_{\text{u0}} + \alpha_{\text{d0}})}{2k_{\text{eff}}} - \frac{\Delta\Phi_{\text{dep}}}{k_{\text{eff}}\, T^2}, \tag{5}$$

with the wave vector independent systematic errors effectively eliminated in real-time.

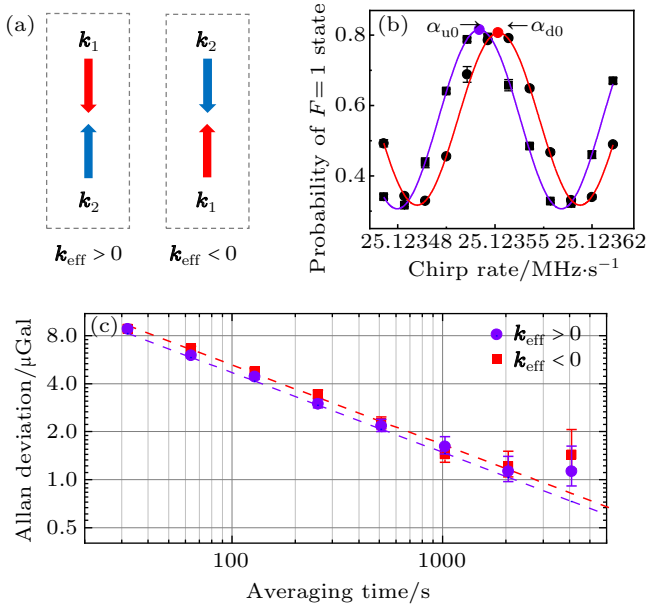


Fig. 3. Continuous g measurement at NIM, started from 2019-01-20T12:17Z. (a) The diagram of the two pairs of Raman beams. If the chirp rate is $-\alpha_{\text{u}}$ ($+\alpha_{\text{d}}$), then $\boldsymbol{k}_{\text{eff}} > 0$ ($\boldsymbol{k}_{\text{eff}} < 0$). (b) Interferometry fringes for the two configurations of $\boldsymbol{k}_{\text{eff}}$. Each of them is obtained by 48 drops in 16 s for chirping up or down. Each black dot is the probability of the atoms in $|1,0\rangle$ state by averaging of 4 drops. The error bars represent the statistical errors. The purple (red) line is the fitting curve according to the chirp rate of $-\alpha_{\text{u}}$ ($+\alpha_{\text{d}}$). (c) Allan deviations of the gravity signal corrected for Earth's tides, in the $\boldsymbol{k}_{\text{eff}} > 0$ (purple) configuration and the $\boldsymbol{k}_{\text{eff}} < 0$ (red) configuration, respectively. The dashed lines indicate the averaging expected for white noise.

The corresponding uncertainty can be derived from the resolutions of the measured g values with $\boldsymbol{k}_{\text{eff}} > 0$ and $\boldsymbol{k}_{\text{eff}} < 0$ configurations, respectively. The Allan deviations of the measured g values that have been corrected by Earth's tides for both configurations are shown in Fig. 3(c). After averaging over 2000 seconds, the resolutions are achieved as $\sigma_{\text{u}} = 1.1$ μGal for $\boldsymbol{k}_{\text{eff}} > 0$ and $\sigma_{\text{d}} = 1.2$ μGal for $\boldsymbol{k}_{\text{eff}} < 0$, respectively. The calibrated uncertainty of the wave vector independent systematic errors can be achieved as $\sigma_g = \frac{1}{2}\sqrt{\sigma_{\text{u}}^2 + \sigma_{\text{d}}^2} \approx 0.8$ μGal.

4.2. Tilting

For the atomic gravimeter, the measured g value is the projection of the real gravitational acceleration on the direction of the Raman lasers. The tilting of the Raman lasers

causes another systematic error of the g value. With the multi-round calibration, the directions of the Raman lasers are precisely adjusted to be parallel to the direction of the gravity.[32] With this method, the systematic error caused by the tilt angles is also effectively eliminated with an uncertainty of $(0, -0.8)$ μGal.

4.3. Two-photon light shift

For real application, the Raman lasers include two pairs of counter-propagating lasers with $\boldsymbol{k}_{\rm eff} > 0$ and $\boldsymbol{k}_{\rm eff} < 0$, respectively, as shown in Fig. 3(a). As the atoms are free falling, the chirp rate α compensates the Doppler shift and keeps one pair of Raman lasers on resonance with the atoms. Whereas the other pair is off-resonant, which induces an additional AC Stack shift for the atoms during the $\pi/2$–π–$\pi/2$ Raman pulses. This effect is called the two-photon light shift (TPLS)[33] and causes a light intensity dependent phase shift in the atom interferometer which biases the measured g value. The phase shift can be expressed as[34]

$$\Delta\Phi_{\rm TP} = \left(\frac{\Omega_{\rm eff}^{(1)}}{4\delta_{\rm D}^{(1)}} - \frac{\Omega_{\rm eff}^{(3)}}{4\delta_{\rm D}^{(3)}}\right), \tag{6}$$

where $\Omega_{\rm eff}^{(i)}$ is the Raman–Rabi frequency which is proportional to the intensity of the Raman lasers and $\delta_{\rm D}^{(i)}$ is the off-resonant Doppler shift for the i-th pulse.

During the evaluation, we change the intensity of the Raman lasers to observe the varying of the measured g value and to find out the corresponding relationship. The result is presented in Fig. 4. For convenience, the Raman–Rabi frequency ratio of 1.0 is set to be $2\pi \times 25.7$ kHz. Linear fit is applied to extract the relationship of the Raman laser intensity and the measurement shift, which gives the slope of 82.5 ± 4.2 μGal.

During the g measurement evaluation, the Raman–Rabi frequency is set to be $2\pi \times 26.6$ kHz and the corresponding g value shift due to the TPLS is 84.3 μGal with uncertainty of 4.3 μGal.

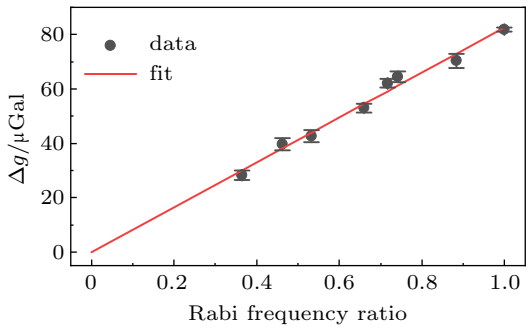


Fig. 4. Variation of the shift of the measured g value due to the TPLS versus the Rabi frequency ratio. Each g value is an average of about 30 minutes. The ratio of 1.0 corresponds to $2\pi \times 25.7$ kHz. The red line is a linear fit of the data.

4.4. Coriolis effect

In the terrestrial reference system which is rotating, a moving object with a velocity $\boldsymbol{v}$ is affected by the Coriolis effect due to the Earth's rotation. The Coriolis force is

$$\boldsymbol{F}_{\rm cor} = 2m\boldsymbol{v} \times \boldsymbol{\Omega}_{\rm E}, \tag{7}$$

where m is the mass of the object, $\boldsymbol{\Omega}_{\rm E}$ is the angular velocity of the Earth. The Coriolis acceleration along the gravity direction is given by

$$\Delta g_{\rm cor} = 2\,|\boldsymbol{v}_{\rm h}||\boldsymbol{\Omega}_{\rm E}|\cos\theta\cos\varphi, \tag{8}$$

where $\boldsymbol{v}_{\rm h}$ is the horizontal velocity of the object, θ is the angle between $\boldsymbol{v}_{\rm h}$ and west direction, φ is the latitude of the location. Note that when the horizontal velocity is along west (east), it will have the largest increasing (decreasing) on the gravitational acceleration, as shown in Fig. 5(a).

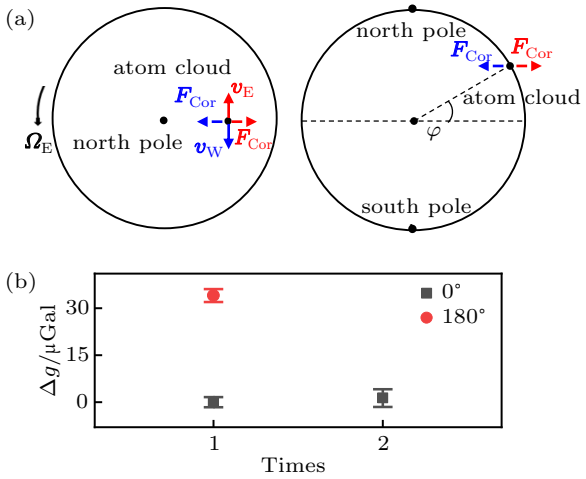


Fig. 5. (a) The schematic of the Coriolis force related to the Earth's rotation. Left: The Earth's top view above the north pole. Right: The Earth's side view parallel to the equator. The blue (or red) arrows represent the horizontal velocity direction $\boldsymbol{v}_{\rm W}$ (or $\boldsymbol{v}_{\rm E}$) of the atom cloud and the corresponding Coriolis force direction. (b) Measured g values for two opposite orientations of the sensor head (0° and 180°).

For an atomic gravimeter, an imbalance in the intensities of the counter-propagating cooling lasers from different directions can cause a horizontal non-zero initial velocity of the atom cloud when it starts falling. No matter which direction of this initial velocity, the Coriolis force will affect the measured g value. The Coriolis effect of an atomic gravimeter can be calibrated by rotating the gravimeter for 180° and back to obtain the difference of the measured g value,[25,35,36] even the initial velocity of the falling atom cloud is unknown.

During the evaluation, we set the atomic gravimeter USTC-AG02 to perform the g measurement (0° orientation). Then, the sensor head was rotated for 180° for another set of g measurement, and turned back to measure again. Before the evaluation of the Coriolis effect, we had adjusted the Raman lasers to be vertical exactly, and the tilt angles of the sensor

head were recorded by the tilt-meters.[32] After a rotation, we adjusted the supporting legs of the sensor head to recover the tilt angles rapidly. The results are shown in Fig. 5(b). The average of these measurements gives the Coriolis effect of $\Delta g_{\rm cor} = -17.0 \pm 1.3$ μGal.

4.5. Self-attraction

From the law of universal gravitation, all components of the gravimeter give attractive forces to the test mass, the atoms. The gravitational field generated by the gravimeter itself gives an additional systematic error term in the g measurement. This term is called the self-attraction effect (SAE). To precisely evaluate the self-attraction effect, the finite element approach is applied. We mesh each component of the gravimeter into numerous elements with very small volumes. The center of 3D-MOT is marked as the origin of coordinate, where the atoms begin falling.

For a series of positions along the atomic trajectory, we calculate the gravitational acceleration in the vertical (z) direction generated by each meshing element, and add them up. The process can be expressed as

$$\Gamma_j \approx G \sum_i \frac{z_{ij}\rho_i V_i}{\left(x_i^2 + y_i^2 + z_{ij}^2\right)^{1.5}}, \tag{9}$$

where Γ_j is the gravitational acceleration in z direction at the $j^{\rm th}$ position induced by the gravimeter itself, G is the gravitational constant, V_i is the volume of the $i^{\rm th}$ element, ρ_i is the density of the $i^{\rm th}$ element, and (x_i, y_i, z_{ij}) is the coordinate of the $i^{\rm th}$ element center.

After figuring out Γ, as shown in Fig. 6(a), we can derive the Lagrangian $\mathcal{L}_{\rm s}$ which is linked to the potential energy of an atom in the gravitational field generated by the gravimeter itself as[37,38]

$$\mathcal{L}_{\rm s} = -\delta E_{\rm s} = m \int \Gamma(z) {\rm d}z = m f(z), \tag{10}$$

where m is the atomic mass, and $f(z)$ is the integrating of Γ over z, as shown in Fig. 6(a).

From the phase difference between the two atomic paths (path A–B–D and path A–C–D), we can calculate the additional acceleration $\Delta g_{\rm s}$ from the SAE with the perturbative path integral method[38]

$$\begin{aligned}\Delta g_{\rm s} = &-\frac{m}{\hbar k_{\rm eff} T^2} \\ &\times \left(\int_{t_1}^{t_1+T} f\left(z_{\rm AB}(t)\right) {\rm d}t + \int_{t_1+T}^{t_1+2T} f\left(z_{\rm BD}(t)\right) {\rm d}t \right. \\ &\left. - \int_{t_1}^{t_1+T} f\left(z_{\rm AC}(t)\right) {\rm d}t - \int_{t_1+T}^{t_1+2T} f\left(z_{\rm CD}(t)\right) {\rm d}t \right),\end{aligned} \tag{11}$$

where $mf\left(z_{\rm AB}(t)\right) = m\int_{\rm A}^{\rm B} \Gamma(z){\rm d}z$ represents the Lagrangian between the atomic positions A and B, $z(t)$ is the atoms center position which takes account the local g and the momentum transferred from $\boldsymbol{k}_{\rm eff}$, $\hbar$ is the reduced Planck constant, and t_1 is the time of the first Raman pulse.

From Eq. (11), considering the contribution from all the components of the gravimeter, we obtain $\Delta g_{\rm s} = 0.4$ μGal. The uncertainty in the calculation mainly comes from the influence of some tiny sub-components which are neglected in the modeling, the meshing fineness, and the imperfect knowledge of the material densities.

For a rough estimation, we deal with the components one by one, and the results are shown in Fig. 6(b). The sum of the SAE contributions equals to 0.4 μGal. The density settings in a proper range are modulated to re-calculated the SAE and we find that the variation is within ±0.1 μGal, which is considered as the global uncertainty of the SAE calculation.

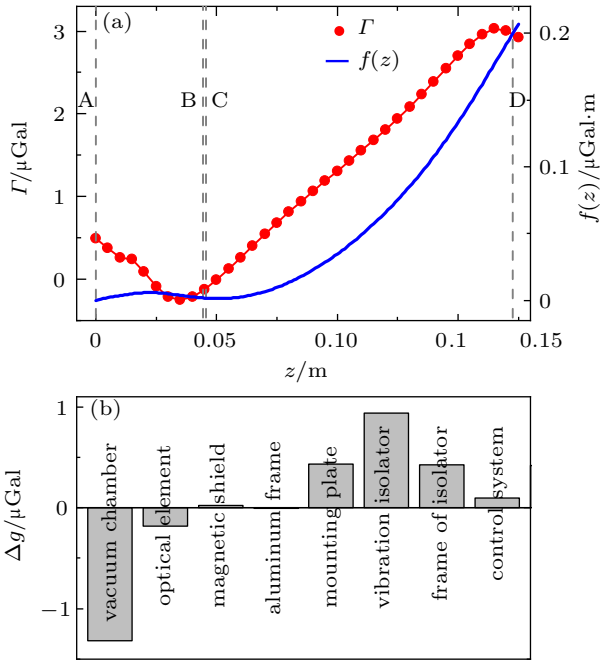


Fig. 6. (a) The figure of the SAE analysis for the entirety of USTC-AG02. We set the 3D-MOT center as $z = 0$. The 4 dashed lines (z = A, B, C, D) represent the atoms center positions at the 3 Raman pulses. The red dots indicate the gravitational acceleration in z direction along the atomic trajectory; the blue line indicates the integration of Γ over z. (b) The SAE contributions of USTC-AG02's all components.

4.6. Gravity gradient

The gravity gradient near the surface of the Earth is around 300 μGal/m in vertical direction. Similar to the analysis of the SAE, the zz-component gravity gradient (T_{zz}) can also be treated as a perturbation, as shown in Fig. 7. Along the atomic trajectory, the perturbation increases linearly. The corresponding Lagrangian $\mathcal{L}_{\rm gg}$ of an atom in the gravitational field can be expressed as

$$\mathcal{L}_{\rm gg} = m \int \Gamma(z) {\rm d}z = m f(z) = m T_{zz} z^2/2, \tag{12}$$

where m is the atomic mass. The Lagrangian $\mathcal{L}_{\rm gg}$ is also set to be zero at the 3D-MOT center ($z = 0$). With Eq. (11), we

obtain $\Delta g_{gg} = 0.051 \times T_{zz}$. It means that the effective measurement point is 0.051 m below the 3D-MOT center, which is independent of the gravity gradient along vertical direction T_{zz}.

For USTC-AG02, the distance between the 3D-MOT center and the ground is 1.078 m, so the effective measurement height is 1.027 m, which is independent of T_{zz}. The error of the height can be controlled to be less than 1 mm, so the corresponding uncertainty is considered as 0.3 μGal. Thus, the systematic error induced by the gravity gradient is evaluated as 0 ± 0.3 μGal.

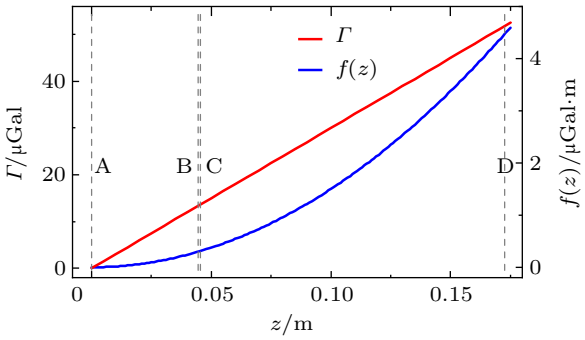


Fig. 7. The calculated influence of the gravity gradient ($T_{zz} \approx 300$ μGal/m) near the surface of the Earth. The red line indicates the perturbation along the atomic trajectory; the blue line indicates the integration of the perturbation over z. The result is independent of T_{zz}, but for the sake of convenience.

4.7. Wave-front distortion

The measured g value can be affected by the difference of the wave-fronts between the two Raman lasers ($\boldsymbol{k}_1$ and $\boldsymbol{k}_2$), which is mainly caused by the imperfection of the retro-reflector of the Raman lasers. A peak-to-valley value of $\lambda/15$ on the mirror surface can induce a bias of about -2 μGal in the g measurement.[30] For the retro-reflector in USTC-AG02, the peak-to-valley value on the surface was manufactured to be less than $\lambda/20$ before mounting. For the mounting, we just placed the mirror on a plane slightly without clamping, so the mechanical strain can be as small as possible. Even though, we consider expanding the uncertainty to 6 μGal, and take 0 as the bias.

4.8. Laser frequency and clock reference

We locked the laser on ^{87}Rb transition line with the magnetic-enhanced MTS. The peak-to-peak variation of the beat frequency is about 160 kHz over 10 hours.[28] So the uncertainty induced by the laser frequency can be estimated as 0.2 μGal.

We used a rubidium clock (SRS FS725S) as the reference clock in our gravimeter. The output frequency of the clock is 10 MHz with an accuracy of 5×10^{-11}, which means the corresponding errors in the g measurement can be negligible.

4.9. Environmental effects

The environmental effects include Earth's tide, air pressure as well as polar motion of the Earth. They are varying with time and affecting the local gravity g, which are needed to be corrected. At the moment of 2019-01-16T16:00Z, which is also the averaging measurement time of USTC-AG02 in NIM, the biases induced by Earth's tide, air pressure, and polar motion are calculated as -43.6 μGal, -5.3 μGal, and -5.4 μGal, respectively.

4.10. Overall and comparison

Table 2 lists the dominant systematic errors of the atomic gravimeter USTC-AG02. The overall bias of g measurement is 67.7 μGal with the uncertainty of ±7.6 μGal. With the reference time of 2019-01-16T16:00Z, the environmental effects give the total contribution of -54.3 μGal with the uncertainty of 0.7 μGal. The total bias induced by all of the effects from the gravimeter itself and the environment is 13.4 ± 7.6 μGal.

Table 2. Systematic errors of the device and the environmental effects budget. The bias of the environmental effects is at the moment of 2019-01-16T16:00Z, in NIM.

Effect	Bias/μGal	Uncertainty/μGal
Wave-vector independent errors	0	0.8
Tilt	0	0.8
Two-photon light shift	84.3	4.3
Coriolis force	−17.0	1.3
Self-attaction effect	0.4	0.1
Gravity gradient	0	0.3
Wave-front distortion	0	6
Laser frequency	0	0.2
Total of the gravimeter	67.7	7.6
Tide	−43.6	0.5
Air pressure	−5.3	0.5
Polar motion	−5.4	0.1
Total of environment	−54.3	0.7
Total	13.4	7.6

Correcting our measured g value with the total bias and considering the statistical uncertainty of 0.8 μGal in the measurement, we finally obtained $g = 980121369.2(15.3)$ μGal at the comparison lab. For achieving the confidence to 95%, the uncertainty of the g value has been expanded to $2\sigma = 15.3$ μGal. A comparison with the reference value $g = 980121365.5$ μGal given by the falling corner cube optical gravimeter NIM-3A shows that the degree of equivalence of USTC-AG02 is $3.7(15.3)$ μGal.

5. Discussion and conclusion

In conclusion, we have built a compact atomic gravimeter USTC-AG02 based on the matter wave interferometry and described its main features and performance. In particular, we have shown the compactness and miniaturization of the gravimeter, which make it easy for the transportation over

1300 km. The size of USTC-AG02 is small compared with the other atomic gravimeters. A continuous g measurement in NIM shows that the measured values agree well with the tide model and the fluctuations of the residues are around ± 10 μGal. A measurement sensitivity of 35.5 μGal/Hz$^{1/2}$ has been achieved, and after averaging over 4000 s, the resolution is about 0.8 μGal. Then, the dominant systematic errors of the gravimeter itself and the environmental effects are evaluated and corrected within a total uncertainty (2σ) of 15.3 μGal. Comparing with the reference g value offered by NIM, USTC-AG02 achieves a DoE of 3.7(15.3) μGal. It means that the compact atomic gravimeter USTC-AG02 can work as an absolute gravimeter with the accuracy in μGal level. Compared to the other atomic gravimeters participating in ICAG-2017, USTC-AG02 is more compact with similar performance, which makes it closer to the field applications.

Acknowledgment

We would like to thank Dr. Shu-Qing Wu, Dr. Qi-Yu Wang and the gravity precision measurement team at NIM for their providing the laboratory for the g measurement and the helps during the calibration.

References

[1] Marson I and Faller J E 1986 *J. Phys. E: Sci. Instrum.* **19** 22
[2] Furuya M, Okubo S, Sun W, Tanaka Y, Oikawa J, Watanabe H and Maekawa T 2003 *Spatiotemporal gravity changes at Miyakejima Volcano*, Japan: Caldera collapse, explosive eruptions and magma movement Journal of Geophysical Research: Solid Earth **108**
[3] Courtenay N de, Darrigol O and Schlaudt O 2019 *The reform of the International System of Units (SI)*: philosophical, historical, and sociological issues (London ; New York, NY: Routledge) p. 131
[4] Wang H, Wu L, Chai H, Hsu H and Wang Y 2016 *IET Radar, Sonar & Navigation* **10** 862
[5] Okubo S, Yoshida S, Sato T, Tamura Y and Imanishi Y 1997 *Geophys. Res. Lett.* **24** 489
[6] Liard J and Gagnon C 2002 *Metrologia* **39** 477
[7] Li C J, Xu J Y, Feng J Y, Su D W and Wu S Q 2015 *Proceedings Volume* 9446*, Ninth International Symposium on Precision Engineering Measurement and Instrumentation*, March 6, 2015, Changsha, China
[8] Peters A, Chung K Y and Chu S 1999 *Nature* **400** 849
[9] Peters A, Chung K Y and Chu S 2001 *Metrologia* **38** 25
[10] Gouet J L, Mehlstaubler T, Kim J, Merlet S, Clairon A, Landragin A and Santos F P D 2008 *Appl. Phys. B* **92** 133
[11] Zhou L, Xiong Z Y, Yang W, Tang B, Peng W C, Wang Y B, Xu P, Wang J and Zhan M S 2011 *Chin. Phys. B* **28** 013701
[12] Bidel Y, Carraz O, Charrière R, Cadoret M, Zahzam N and Bresson A 2013 *Appl. Phys. Lett.* **102** 144107
[13] Wang Q Y, Wang Z Y, Fu Z J and Lin Q 2016 *Chin. Phys. B* **25** 123701
[14] Karcher R, Imanaliev A, Merlet S and Santos F P D 2018 *New J. Phys.* **20** 113041
[15] Huang P W, Tang B, Chen X, Zhong J Q, Xiong Z Y, Zhou L, Wang J and Zhan M S 2019 *Metrologia* **56** 045012
[16] Wu X, Pagel Z, Malek B S, Nguyen T H, Zi F, Scheirer D S and Müller H 2019 *Sci. Adv.* **5** 9
[17] Hu Z K, Sun B L, Duan X C, Zhou M K, Chen L L, Zhan S, Zhang Q Z and Luo J 2013 *Phys. Rev. A* **88** 043610
[18] Gillot P, Francis O, Landragin A, Santos F P D and Merlet S 2014 *Metrologia* **51** 5
[19] Freier C, Hauth M, Schkolnik V, Leykauf B, Schilling M, Wziontek H, Scherneck H G, Müller J and Peters A 2016 *J. Phys.: Conf. Ser.* **723** 012050
[20] Mcguinness H J, Rakholia A V and Biedermann G W 2012 *Appl. Phys. Lett.* **100** 011106
[21] Bidel Y, Zahzam N, Blanchard C, Bonnin A, Cadoret M, Bresson A, Rouxel D and Lequentrec-Lalancette M F 2018 *Nat. Commun.* **9** 627
[22] Jiang Z, Pálinkáš V, Arias F E, *et al.* 2012 *Metrologia* **49** 666
[23] Francis O, Baumann H, Ullrich C,, *et al.* 2015 *Metrologia* **52** 07009
[24] Wu S Q, Feng J Y, Li C J, *et al.* 2020 *Metrologia* **57** 07002
[25] Wang S K, Zhao Y, Zhuang W, Li T C, Wu S Q, Feng J Y and Li C J 2018 *Metrologia* **55** 360
[26] Fu Z F Z, Wang Q W Q, Wang Z W Z, Wu B W B, Cheng B C B and Lin Q L Q 2019 *Chin. Opt. Lett.* **17** 011204
[27] Chen B, Long J B, Xie H T, Chen L K, and Chen S 2019 *Acta Phys. Sin.* **68** 183301 (in Chinese)
[28] Long J B, Yang S J, Chen S and Pan J W 2018 *Opt. Express* **26** 27773
[29] *Draft_Technical Protocol of CCM.G-K2.2017 and Pilot Study*-5.1 version
[30] Louchet-Chauvet A, Farah T, Bodart Q, Clairon A, Landragin A, Merlet S and Santos F P D 2011 *New J. Phys.* **13** 065025
[31] Cheng B, Gillot P, Merlet S and Santos F P D 2015 *Phys. Rev. A* **92** 063617
[32] Xie H T, Chen B, Long J B, Xue C, Chen L K and Chen S 2019 *Chin. Phys. B* **29** 073701
[33] CladéP, Mirandes E D, Cadoret M, Guellati Khélifa S, Schwob C, Nez F, Julien L and Biraben F 2006 *Phys. Rev. A* **74** 052109
[34] Gauguet A, Mehlstäubler T E, Lévèque T, Gouët J L, Chaibi W, Canuel B, Clairon A, Santos F P D and Landragin A 2008 *Phys. Rev. A* **78** 043615
[35] Wu B, Zhu D, Cheng B, Wu L, Wang K, Wang Z, Shu Q, Li R, Wang H, Wang X and Lin Q 2019 *Opt. Express* **27** 11252
[36] Farah T, Gillot P, Cheng B, Landragin A, Merlet S and Santos F P D 2014 *Phys. Rev. A* **90** 023606
[37] Storey P and Cohen-Tannoudji C 1994 *Journal De Physique II* **4** 1999
[38] Dagostino G, Merlet S, Landragin A and Santos F P D 2011 *Metrologia* **48** 299